Thermal Performance of an Integrated Heat Spreader for GaN HEMT devices

Ahmad, Faheem; Aunsborg, Thore Stig; Beczkowski, Szymon; Munk-Nielsen, Stig; Jørgensen, Asger Bjørn

Published in:
Proceedings of CIPS 2022 - 12th International Conference on Integrated Power Electronics Systems

Publication date:
2022

Document Version
Accepted author manuscript, peer reviewed version

Thermal Performance of an Integrated Heat Spreader for GaN HEMT devices

Faheem Ahmad[a], Thore Stig Aunsborg[a], Szymon Michal Beczkowski[a], Stig Munk-Nielsen[a] and Asger Bjørn Jørgensen[a]
[a]AAU Energy, Aalborg University, Aalborg, Denmark.

Abstract

Utilizing the fast switching speed of gallium nitride (GaN) devices requires compact and low inductive printed circuit board (PCB) layouts. A heatsink is mounted to operate the GaN devices at high power. However, auxiliary components such as DC-link capacitors or gate drivers must be moved out of proximity or to the other side of the PCB to fit the heatsink. This paper analyses an integrated heat spreader solution which provides flexibility in designing an optimized electrical layout as well as providing thermal performance that is comparable to conventional thermal-pad with a flat heatsink cooling method.

1 Introduction

Wide bandgap (WBG) devices are improving with smaller junction capacitance and low package inductance. 600-650V GaN devices have been reported to achieve dv/dt upwards of 100V/ns [1]. Such voltage transition speed and clean switching is dependent on good layout with minimized parasitics. Multilayer PCBs allow for flexibility in electrical layout [2]. However, their thermal performance is poor when compared to insulated metal substrate (IMS) and direct bonded copper (DBC) based designs [3]. To solve this issue GaN device packages with top-side cooling have been shown to utilize PCB/DBC combination to achieve high thermal performance while electrical layout is kept on PCB taking advantage of multilayer design [4]. Nevertheless, good layout often requires DC link capacitor and gate driver be placed in close proximity with the device and given small package of GaN devices, it becomes difficult to properly attach a heatsink as shown in Figure 1(a).
Instead of utilizing a flat surfaced heatsink, this paper analyses heatsink with cavity machined into it. The cavity is then filled with different thermal compounds. This enables varying height components to be placed inside the machined cavity. The concept is shown in Figure 1(b) and is referred to as integrated heat spreader. The integrated heat spreader potentially provides heat extraction for all the components i.e. gate drivers, linear voltage regulators etc.
This paper investigates thermal performance of conventional method of a thermal-pad with a flat heatsink, conducting heat directly from top-side GaN high-electron-mobility transistor (HEMT). This is compared to the integrated heat spreader solution where GaN HEMT is embedded into a thermal compound. Both commercial thermal compounds and in-house mixtures are tested. Furthermore, impact of various heights of the machined cavity is also presented. Finally, finite element analysis (FEA) on 3D geometry of the experimental setup will be conducted in COMSOL Multiphysics 5.6 to assist in understanding the observed results.

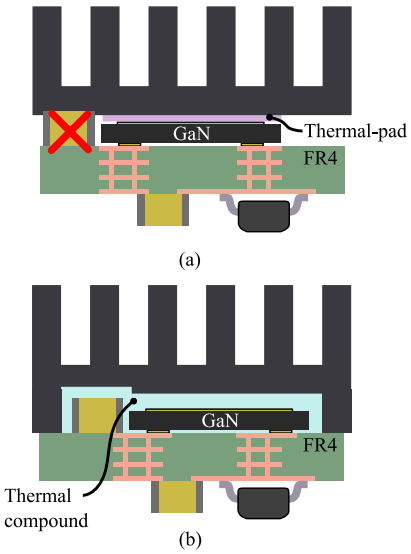

Figure 1: Cooling of GaN components by (a) conventional flat heatsink limiting height of neighbour components and (b) an integrated heat spreader with more flexibility of layout.

2 Thermal Interface Material

Heatsinks attached for cooling semiconductor devices do not provide a perfect contact with the device due to

surface roughness. This leads to formation of air-gaps between the device and heatsink surface. To overcome this, thermally conductive thermal interface materials (TIM) are used to fill the gap between device package and heatsink surface. TIM comes in several forms such as pads, gels and liquid gap fillers.

In this paper, for conventional method of flat heatsink, a 0.5mm thick Gap-pad is used. Thermal conductivity of Gap-pad is 5W/m·K [5]. For the integrated heat spreader solution, two different thermal compound are tested. Filler A is a two-component liquid gap filler of conductivity 3.6W/m·K [6]. Filler B is a hardening resin with thermal conductivity of 1.5W/m·K [7]. Given low thermal conductivity of Filler B, authors added 10% by volume Aluminium Nitride (AlN) powder (particle size distribution D50 of 7-11μm) in it [8]. Tests are conducted on this mixture, termed as Filler C(B + 10% AlN). Higher concentration of AlN made the mixture non-workable due to high viscosity. A summarized table of thermal conductivity and dielectric strength of different TIM is provided in Table 1. Thermal conductivity of Filler C(B + 10% AlN) will be measured through experiment whereas its dielectric strength is not ascertained in this paper.

Table 1: PROPERTIES OF TIM

TIM	Thermal Cond. (W/m·K)	Diele. Strength (V/mil)
Gap-pad [5]	5	254
Filler A [6]	3.6	275
Filler B [7]	1.5	388
Filler C	To be meas.	–

3 Methodology

For testing the two cooling methodologies a dual half-bridge PCB layout is used for the experiments. Designed PCB is 4 layer 70mm x 70mm in dimension. Gate drivers and DC link capacitors are designed to be placed on the opposite side of PCB than GaN devices. This reduces additional thermal coupling paths and isolated impact of TIM from GaN device to heatsink can be studied. The PCB is populated with only GaN HEMT devices (GS66506T). A BGA heatsink (CMBA024949) made of Al 6063 material is utilized for both methodologies. For the integrated heat spreader method a cavity is machined in the heatsink. The GaN HEMT has a device thickness of 0.54mm. At 0.06mm of solder layer thickness, the total height of GaN HEMT from PCB is 0.6mm. An integrated heat spreader with 1.7mm deep cavity when placed over the HEMT allows 1.1mm of thermal compound thickness on top of the GaN device. Therefore, further heat spreader are tested at reduced cavity depth of 1.3mm and 1.0mm which gives 0.7mm and 0.4mm thick thermal compound respectively.

3.1 Experiment Results

To dissipate power, one HEMT gate is applied with $V_{GS(ON)}$ voltage of 6V and a fixed drain current of 8A is sourced through it. At 67mΩ $R_{DS(ON)}$ a constant conduction loss of 4.3W is induced in the device. A 24V/3.6W fan is kept at a distance of 6cm from heatsink. Power is continuously dissipated in the device for 100s while temperature reaches steady state. Opsens fibre optic temperature sensor is used to measure the device temperature through a pinhole in PCB [9]. According to GaN Systems, under normal device temperature operating range, the difference between device junction temperature and package temperature is close to 1°C [10]. This has been corroborated by detailed FEM simulation of GaN Systems device as conducted in [11]. Figure 2 shows setup with integrated heat spreader. Excess thermal compound is coming out of via when the integrated heat spreader is applied, suggesting the GaN HEMTs are completely embedded in thermal compound.

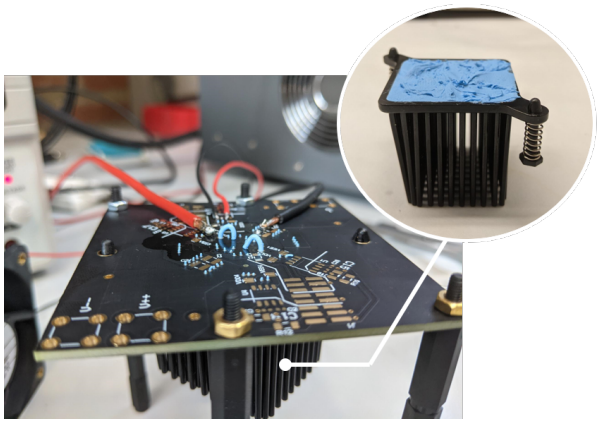

Figure 2: Experiment setup with integrated heat spreader.

Shown in Figure 3(a) are the temperature measurement for different solutions. Gap-pad shows best performance with lowest temperature. Filler A is tested at all three cavity depth. However it performs best at 1.0mm cavity depth. It is to be noted that Filler A (at 1.0mm cavity depth) even with lower conductivity performs comparably to the Gap-pad. Filler B is not tested as it is a hardening resin and it will render the PCB unusable afterwards. Also Filler B thermal conductivity is given in datasheet and is lower than Filler A. Therefore, the authors decided to test Filler C which is an in-house mixture. Since Filler A performed best at 1.0mm cavity depth, Filler C was only tested at 1.0mm cavity depth of integrated heat spreader.

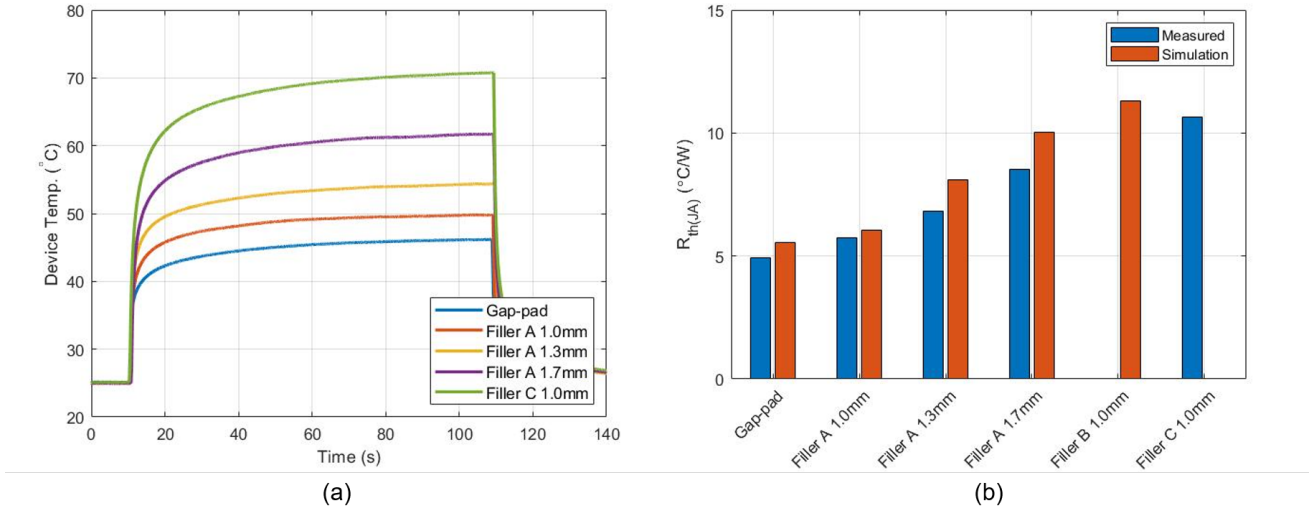

Figure 3: (a) DUT temperature in different solution at 4.3W of loss, (b) Thermal resistance $R_{th(JA)}$ based on measured as well as FEM simulation.

By embedding the GaN HEMT in a thermal compound, integrated heat spreader methodology was anticipated to perform slightly better than the flat heatsink solution. This is because the thermal compound in heat spreader envelops the entire GaN HEMT package, which allows for additional surface area to dissipate heat. This is represented by additional thermal component $R_{th(JP)}$, $R_{th(PS)}$ in Figure 5(b) which are junction-package and package-heatsink thermal resistance respectively. But the results did not support this hypothesis. Furthermore, Filler C registered highest device temperature. A discussion on Filler C result is presented at the end of this paper. In next section a finite element method (FEM) simulation is conducted to improve the understanding of the observed results.

3.2 Modeling and FEM Simulation

The GaNPX package for GaN Systems top side cooled devices have a major heat transfer path through its top pad [10]. The large contact area between the semiconductor substrate and top pad is shown in Figure 4. Thus, the GS66506T datasheet provides only the thermal resistance from junction-case (top side) ($R_{th(JC)}$). In Figure 5 thermal resistance network from the GaN HEMT device to ambient is provided for both flat heatsink and integrated heat spreader method. $R_{th(CS)}$ represents thermal resistance of either the thermal-pad in flat heatsink or the thermal compound in integrated heat spreader in Figure 5(a), (b) respectively. $R_{th(SA)}$ is heatsink-ambient thermal resistance. For both flat heatsink and integrated heat spreader method a downward heat conduction path through the PCB is also present. This includes the junction-board ($R_{th(JB)}$) and board-ambient

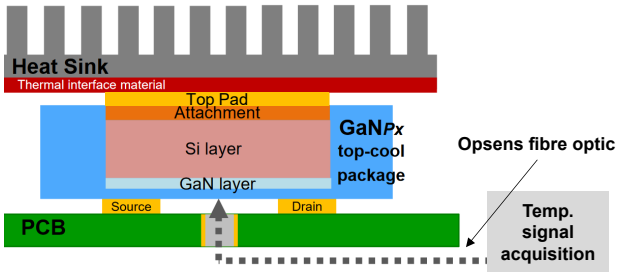

Figure 4: Structure of GaNPX package for GaN Systems top side cooled devices [10].

($R_{th(BA)}$) thermal resistance. In addition, for integrated heat spreader a direct contact between PCB and heatsink also exists through the thermal compound. This is shown by $R_{th(BS)}$ in Figure 5(b).

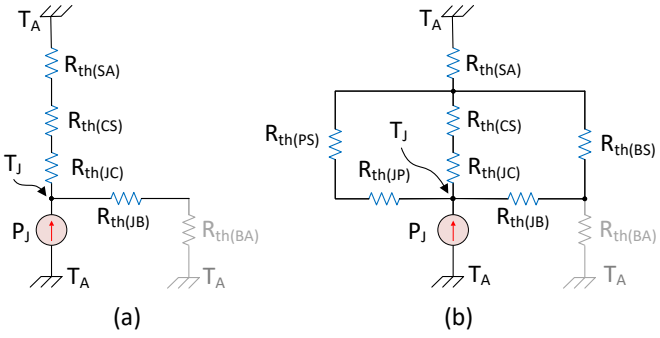

Figure 5: Thermal resistance network of heat conduction path from junction to ambient in (a) flat heatsink method, and (b) integrated heat spreader method. Greyed out component shows insulating boundary condition setup in COMSOL.

The 3D geometry of experimental setup which includes PCB, GaN HEMT and heatsink are all included in COMSOL Multiphysics for FEM analysis. The GaN HEMT's 3D geometry is a STEP file provided by the manufacturer. The STEP file contains 3D bodies of external features of GaN HEMT such as top or bottom pads. The internal structure of GaN layer on silicon substrate and its connectivity with the pad is not defined in the STEP model. In the absence of internal semiconductor substrate features, top pad of the GaN HEMT is defined as heat source in COMSOL. An exploded view of the HEMT device is presented in Figure 6.

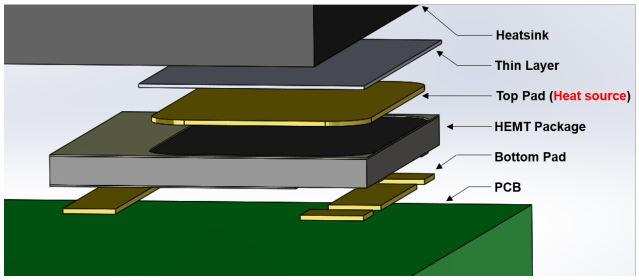

Figure 6: Exploded view of different layers as defined in COMSOL Multiphysics.

Since the top pad is defined as heat source a thin layer is added between it and heatsink as shown in Figure 6. For the flat heatsink methodology, $R_{th(JC)}$ and $R_{th(CS)}$ are modeled within this thin layer. In case of integrated heat spreader methodology only $R_{th(JC)}$ is modeled within this thin layer. The rest of thermal resistance are calculated by COMSOL based on material definition. The heatsink is defined as Al 6063 material with thermal conductivity of 201W/m·K. The HEMT package is defined as silica glass material with a thermal conductivity of 1.38W/m·K. And the PCB as FR4 at 0.3W/m·K of thermal conductivity. Copper is defined for trace as well as device pads.

In this paper the focus is to measure the efficiency of TIM to conduct heat from device to heatsink in two different methodologies. Therefore the PCB surface have been defined as thermally insulating in COMSOL, depicted by greyed out $R_{th(BA)}$ in Figure 5. It is still important to include the PCB as it creates thermal coupling paths between the devices through copper traces [12], [13]. Forced air cooling on heatsink can be modeled with heat transfer coefficient (h-coefficient) value between 300-2000W/m^2·K [14]. For this simulation heatsink boundary has been set to h-coefficient value of 1500W/m^2·K.

Given the small dimension of domains such as vias in PCB as well as thin features in 3D model of GaN HEMT, fine mesh elements are defined for the geometry as shown in Figure 7(a). Figure 7(b) is temperature distribution of GaN HEMT device under flat heatsink methodology. The temperature color legend is restricted from 47°C to 49.5°C. This shows a temperature gradient of around 2°C from the edges to the center region of top pad. Therefore, instead of picking a single point temperature value, a volumetric average of the top pad is estimated. Table 2 shows the volumetric average temperature of the top pad in COMSOL for different cooling methodologies.

Table 2: VOLUMETRIC AVERAGE TEMPERATURE OF TOP PAD IN COMSOL

	Gap-pad	Filler A			Filler B
		1.0mm	1.3mm	1.7mm	1.0mm
°C	48.9	51.0	59.8	68.1	73.7

Figure 3(b) shows final calculation for junction-ambient thermal resistance ($R_{th(JA)}$) using both experimental measurement and FEM simulation. For the Gap-pad and Filler A, simulation results are closely following experimental value within an error of 5-15%. This suggests that the FEM simulation setup has been successful in modeling both flat heatsink and integrated heat spreader methodologies. For Filler B only FEM simulation is conducted as its thermal conductivity is known from datasheet. Simulation results for Filler B are close to experimental measurement of Filler C(B + 10% AlN). Further discussion on Filler C is presented in next section.

Instead of defining the top pad as the heat source, another method could have been defining the HEMT package as heat source. This would have worked well with flat heatsink solution but in case of the integrated heat spreader the surrounding thermal compound will come in direct contact with heat source on the sides of HEMT package leading to additional heat flux path towards heatsink which would be incorrect. Another method to ensure uniformity between the two simulation environment as well as actual experiment is to define semiconductor substrate geometry inside the HEMT package close to top pad as done in [11]. Although more precise, defining detailed HEMT geometry will lead to extremely fine features increasing mesh elements and computation cost.

4 Discussion on Filler C

Filler A has good thermal conductivity of 3.6W/m·K for its price value. Thermal interface materials with much higher thermal conductivity of >15W/m·K are available, but they are expensive. Therefore the authors decided to understand whether high thermal conductivity can be achieved by mixing AlN powder in a relatively inexpensive thermal compound. This is why Filler C was devel-

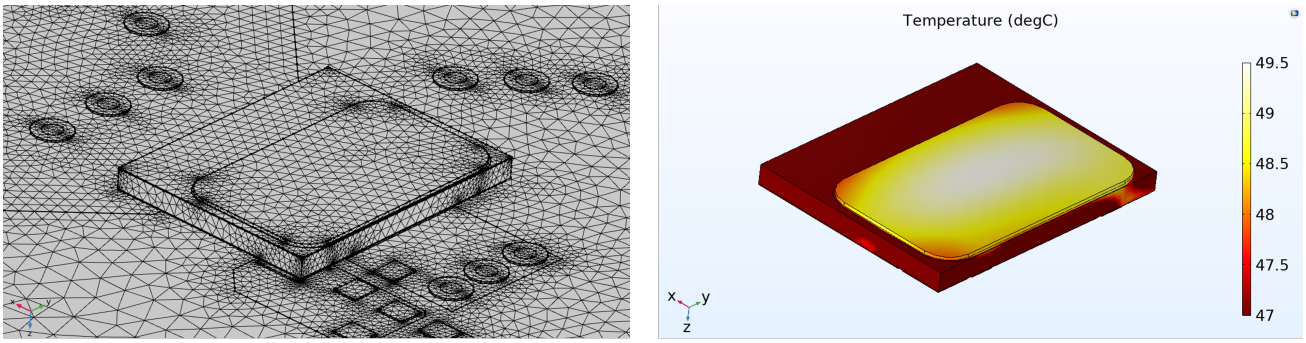

Figure 7: (a) High density of mesh elements defined around thin features like edges and vias, (b) GaN HEMT temperature distribution at $P = 4.3$W on heat source, $h = 1500$W/m^2·K on heatsink surface, and $T_A = 25°$C in flat heatsink methodology.

oped by adding AlN (7-11μm 10%) in a thermally conductive hardening resin (Filler B). Thermal resistance of Filler B calculated from FEM simulation, differ by 6% compared to experimental measurement of Filler C. This is well within the error percentage range that was observed for Gap-pad and Filler A. This suggests that the thermal conductivity of Filler C is very close to its major component Filler B. And therefore the addition of 10% AlN has had an imperceptible impact on Filler B thermal conductivity.

Imperceptible impact of AlN powder on Filler B's thermal performance can be due to its low concentration, AlN particle size distribution or the saturation level of Filler B. Previous research has looked at thermal conductivity of composite mixtures of AlN with different matrix materials [15], [16]. In [15] AlN particles of diameter less than 10μm are mixed in polysterene (PS) of particle size 2mm and 0.15mm. In this work, larger size of PS particles performed better than smaller counterparts at AlN volumetric fraction of 15% or more. At 10% vol. concentration of AlN, base thermal conductivity of PS increased from 0.15W/m·K to 0.27W/m·K. The maximum value of 1W/m·K was achieved at 40% volumetric fraction. In [16], instead of just one filler component both AlN and Al_2O_3 (aluminium oxide) ceramic material is mixed in epoxy. The minimum filler content the paper has presented is at 42.2% (vol.). At this filler content the thermal conductivity of matrix epoxy increased from 0.2W/m·K to 1W/m·K when the ratio of AlN to Al_2O_3 is 1:0. As the fraction of Al_2O_3 is increased the thermal conductivity drops. The paper presents that larger particle size of filler material helps in improving thermal conductivity by reducing the amount (or the area) of the interfaces. The paper achieved a maximum thermal conductivity of 3.4W/m·K from a base value of 0.2W/m·K of matrix epoxy at 58.4% of filler content.

Compared to the thermal conductivity of matrix material presented in [15], [16], Filler B has a high conductivity of 1.5W/m·K and probably the reason for its high viscosity. Therefore adding AlN powder more than 10% by volume was a difficult process. At such low filler content it is accurate to observe that Filler C performs almost similar to Filler B.

5 Conclusion

This paper investigates the thermal performance of an integrated heat spreader solution and compares it to flat heatsink solution. Results show that liquid thermal compound (Filler A) at 1.0mm cavity depth of integrated heat spreader has thermal resistance of 5.7°C/W, which is 17% higher than thermal resistance of Gap-pad in flat heatsink at 4.9°C/W. The Gap-pad performs better owing to its higher thermal conductivity. However, the heat spreader can be machined to house varying height of components such as DC link capacitors or gate drivers which provides flexibility in designing good electrical layout. This will also help in heat extraction from these components. In addition, an in-house mixture (Filler C) of AlN powder with thermally conductive resin (Filler B) is also tested whose performance was significantly worse than Filler A. This is due to the fact that Filler B has low thermal conductivity to begin with and therefore not suitable for this application. Furthermore the volumetric content of AlN powder was too low to have any significant impact on Filler B as seen in previous research works. Based on the experience from this work, authors postulate that it is difficult to come up with in-house mixture that can surpass commercial gels/liquid fillers with high thermal conductivity. For future work, it will be interesting to look into the EMI performance of integrated heat spreader in fast switching WBG devices.

6 Literature

[1] Z. Xu, W. Zhang, F. Xu, F. Wang, L. M. Tolbert, and B. J. Blalock, "Investigation of 600V GaN HEMTs for high efficiency and high temperature applications," *2014 IEEE Applied Power Electronics Conference and Exposition - APEC 2014*, pp. 131–136, 2014.

[2] B. Sun, K. L. Jørgensen, Z. Zhang, and M. A. E. Andersen, "Multi-physic Analysis for GaN Transistor PCB layout," *2019 IEEE Applied Power Electronics Conference and Exposition (APEC)*, pp. 3407–3413, 2019.

[3] J. L. Lu, D. Chen, and L. Yushyna, "A high power-density and high efficiency insulated metal substrate based GaN HEMT power module," *2017 IEEE Energy Conversion Congress and Exposition (ECCE)*, pp. 3654–3658, 2017.

[4] A. B. Jørgensen, S. Bęczkowski, C. Uhrenfeldt, N. H. Petersen, and S. Munk-Nielsen, "A Fast-Switching Integrated Full-Bridge Power Module Based on GaN eHEMT Devices," *IEEE Transactions on Power Electronics*, vol. 34, no. 3, pp. 2494–2504, 2019.

[5] The Bergquist Company: Gap Pad 5000S35. Accessed: August 15, 2021. [Online]. Available: https://www.farnell.com/datasheets/1323705.pdf

[6] Bergquist: BERGQUIST GAP FILLER TGF 3600. Accessed: August 15, 2021. [Online]. Available: https://www.mouser.dk/datasheet/2/48/TGF_3600_EN-1534597.pdf

[7] COOLMAG 29 LV: Thermally Conductive Compound. Accessed: November 28, 2021. [Online]. Available: https://coolmag.net/app/uploads/tds-coolmag-29-lv-en-v0-4-1.pdf

[8] Hoganas: Aluminium Nitride Grade A. Accessed: November 28, 2021. [Online]. Available: https://www.hoganas.com/globalassets/download-media/stc/PD-5168.pdf

[9] OTG-F Fibre Optice Temperature Sensor. Accessed: December 8, 2021. [Online]. Available: https://opsens-solutions.com/wp-content/uploads/sites/4/2015/02/IMP0050-OTG-F-Rev1.9.pdf

[10] GN002 Application Note - Thermal Design GaNPX®Packaged Devices. Accessed: November 20, 2021. [Online]. Available: https://gansystems.com/wp-content/uploads/2021/10/GN002_Thermal-Design-Guide-for-Top-Side-Cooled-GaNpx_T-Devices_Rev-210720.pdf

[11] S. Song, S. Munk-Nielsen, and C. Uhrenfeldt, "How Can a Cutting-Edge Gallium Nitride High-Electron-Mobility Transistor Encounter Catastrophic Failure Within the Acceptable Temperature Range?" *IEEE Transactions on Power Electronics*, vol. 35, no. 7, pp. 6711–6718, 2020.

[12] A. B. Jørgensen, T.-H. Cheng, D. Hopkins, S. Beczkowski, C. Uhrenfeldt, and S. Munk-Nielsen, "Thermal Characteristics and Simulation of an Integrated GaN eHEMT Power Module," in *2019 21st European Conference on Power Electronics and Applications (EPE '19 ECCE Europe)*, 2019, pp. P.1–P.7.

[13] B. Li, K. Wang, H. Zhu, Y. Xie, X. Yang, and L. Wang, "A Double-Sided Cooling GaN Power Module with High Thermal Performance," in *2020 IEEE 9th International Power Electronics and Motion Control Conference (IPEMC2020-ECCE Asia)*, 2020, pp. 2167–2172.

[14] C. Qian, A. M. Gheitaghy, J. Fan, H. Tang, B. Sun, H. Ye, and G. Zhang, "Thermal Management on IGBT Power Electronic Devices and Modules," *IEEE Access*, vol. 6, pp. 12 868–12 884, 2018.

[15] S. Yu, P. Hing, and X. Hu, "Thermal conductivity of polystyrene–aluminum nitride composite," *Composites Part A: Applied Science and Manufacturing*, vol. 33, no. 2, pp. 289–292, 2002.

[16] S. Choi and J. Kim, "Thermal conductivity of epoxy composites with a binary-particle system of aluminum oxide and aluminum nitride fillers," *Composites Part B: Engineering*, vol. 51, pp. 140–147, 2013.